

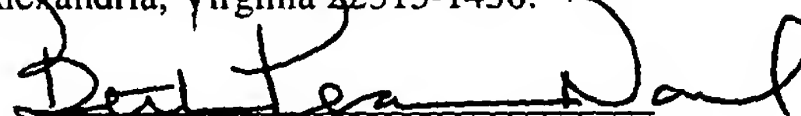
EXPRESS MAIL CERTIFICATE

"EXPRESS MAIL" LABEL **EL978749326 US**

Date of Deposit: August **25**, 2003

I hereby certify that this paper or fee is being deposited with the United States Postal Service "Express Mail Post Office to Addressee" service under 37 CFR 1.10 on the date indicated above, addressed to:

Commissioner of Patents and Trademarks P. O. Box 1450, Alexandria, Virginia 22313-1450.


Beth Pearson-Naul

APPLICATION FOR UNITED STATES LETTERS PATENT

FOR

**DEEP RESISTIVITY TRANSIENT METHOD FOR MWD APPLICATIONS
USING ASYMPTOTIC FILTERING**

**Inventors: Alexander Bespalov
Spring, Texas**

**Michael Rabinovich
Houston, Texas**

**Leonty A. Tabarovsky
Cypress, Texas**

Assignee: Baker Hughes Incorporated

BACKGROUND OF THE INVENTION

1. Field of the Invention

[0001] The invention is related to the field of electromagnetic induction well logging for determining the resistivity of earth formations penetrated by a wellbore. More specifically, the invention relates to measuring the transient signals in an induction tool having a metallic pipe with finite, non-zero and high conductivity.

2. Description of the Related Art

[0002] Electromagnetic induction resistivity instruments can be used to determine the electrical conductivity of earth formations surrounding a wellbore. An electromagnetic induction well logging instrument is described, for example, in U.S. Pat. No. 5,452,761 issued to Beard et al. The instrument described in the *Beard '761* patent includes a transmitter coil and a plurality of receiver coils positioned at axially spaced apart locations along the instrument housing. An alternating current is passed through the transmitter coil. Voltages which are induced in the receiver coils as a result of alternating magnetic fields induced in the earth formations are then measured. The magnitude of certain phase components of the induced receiver voltages are related to the conductivity of the media surrounding the instrument.

[0003] The development of deep-looking electromagnetic tools has a long history. Such tools are used to achieve a variety of different objectives. Deep looking tools attempt to measure the reservoir properties between wells at distances ranging from tens

to hundreds of meters (ultra-deep scale). There are single-well and cross-well approaches, most of which are rooted in the technologies of radar/seismic wave propagation physics. This group of tools is naturally limited by, among other things, their applicability to only high resistivity formations and the power available down-hole.

[0004] At the ultra-deep scale, a technology may be employed based on transient field behavior. The transient electromagnetic field method is widely used in surface geophysics. Examples of transient technology are seen, for example, in Kaufman et al., 1983, "Frequency and transient soundings", Elsevier Science.; Sidorov et al., 1969, "Geophysical surveys with near zone transient EM." Published by NVIGG, Saratov, Russia.; and Rabinovich et al., 1981, "Formation of an immersed vertical magnetic dipole field": *J. Geologiya I Geofizika*, N 3. Typically, voltage or current pulses that are excited in a transmitter initiate the propagation of an electromagnetic signal in the earth formation. Electric currents diffuse outwards from the transmitter into the surrounding formation. At different times, information arrives at the measurement sensor from different investigation depths. Particularly, at a sufficiently late time, the transient electromagnetic field is sensitive only to remote formation zones and does not depend on the resistivity distribution in the vicinity of the transmitter (see Kaufman et al., 1983). This transient field is especially important for logging. A comprehensive study of deep-reading transient EM in wireline measurements has been conducted and discussed by Geldmacher et al., 1997 ("Single well (deep-reading) EM system." Report on the pre-feasibility study, Western Atlas, Inc.). Use of a symmetric logging tool using transient field measurements for formation detection is discussed in U.S. Patent No. 5,530,359, issued to Habashy et al.

[0005] U.S. Patent No. 5,955,884, issued to Payton et al. discusses methods for measuring transient electromagnetic fields in rock formations. Electromagnetic energy is applied to the formation at selected frequencies and waveforms that maximize the radial depth of penetration of the magnetic and electric energy. Payton '884 comprises at least one electromagnetic transmitter and at least one electric transmitter for applying electric energy. The transmitter ands may be either single-axis or multi-axis electromagnetic and/or electric transmitter. In one embodiment the TEM transmitters and TEM receivers are separate modules that are spaced apart and interconnected by lengths of cable, with the TEM transmitter and TEM receiver modules being separated by an interval of one meter up to 200 meters as selected. Radial depth of investigation is related to the skin depth $\delta = \sqrt{2/\sigma\mu\omega}$ which in turn is related to frequency. Lower frequency signals can increase the skin depth. Similarly, the conductivity of the surrounding material inversely affects the skin depth. As conductivity increases the depth of investigation decreases. Finite conductivity casing of the apparatus therefore can reduce the depth of investigation.

[0006] Rapidly emerging measurement-while-drilling (MWD) technology introduces a new, meso-deep (3-10 meters) scale for an electromagnetic logging application related to well navigation in thick reservoirs. The major problem associated with the MWD environment is the introduction of a metal drill pipe close to the area being measured. This pipe produces a very strong response and significantly reduces the sensitivity of the measured EM field to the effects of formation resistivities and remote boundaries. The only previous solution for this problem has been to create a large spacing (up to 20

meters) between transmitter and receiver (as discussed in U.S. Patent No. 6,188,222 B1, issued to Seydoux et al.). The sensitivity of such a tool to remote boundaries is low. Currently, Stolar Horizon, Inc. is developing drill string radar, DSR, for CBM (Coal Bed Methane) wells. DSR provides 3-D imaging within a close range of the wellbore.

[0007] There is a need for a method of processing data acquired with real MWD tools having finite non-zero conductivity in transient field studies. The present invention satisfies this need.

SUMMARY OF THE INVENTION

[0008] The present invention is a method of obtaining a parameter of interest of an earth formation using a tool having a body with finite, non-zero conductivity. The parameter of interest is typically a resistivity of the formation or a distance to a bed boundary in the formation. The method obtains a signal from the earth formation that is substantially independent of the conductivity of the tool. A first signal is produced using a transmitter on the tool. An axially separated receiver receives a second signal that results from an interaction of the first signal with the earth formation. The second signal is dependent on the conductivity of the induction tool. This second signal can be represented using a Taylor series expansion in one half of odd integer powers of time. The $t^{-1/2}$ and $t^{-3/2}$ terms are typically due to the finite-conductivity pipe. The $t^{-5/2}$ term is dominated by the effects of the formation. At least one leading term of the Taylor series expansion can be subtracted from the second signal to reduce the effect of the metal pipe.

[0009] A filtering operation is applied to the second signal. In one mode of the invention, a differential filtering operation is employed. A typical differential filter further comprises taking a time-derivative of the product of the second signal with $t^{1/2}$. Such filter eliminates the main term of the pipe contribution to the signal. In an alternate mode of the invention, an integral filtering operation is employed. Such an integral filtering operation can further comprise defining a first and second specified time, t_1 and t_2 . An average of the measured field with a weight of $t^{1/2}$ can be made over two time intervals center on the first and second specified times, both intervals having a duration Δ . A difference produces an integration filter:

$$I_1 - I_2 \approx \frac{1}{\Delta} \int_{-\Delta/2}^{\Delta/2} t^{1/2} [H_z(t - t_1) - H_z(t - t_2)] dt$$

where H_z represents the second signal. Such a filter eliminates most of the influence of the pipe.

BRIEF DESCRIPTION OF THE DRAWINGS

[0010] FIG. 1 (Prior Art) shows an induction logging instrument as it is typically used to make measurements suitable for use with the method of the invention.

FIG. 2A shows a typical cylindrical wellbore configuration for oil exploration.

FIG. 2B shows the wellbore from Figure 2A introducing a perfectly conductive pipe.

FIG. 3 shows a transmitter-receiver assembly positioned near a formation boundary.

FIG. 4 shows transient responses due to a remote plane boundary of the configuration of Fig. 3.

FIG. 5 shows a cylindrical model of the borehole configuration.

FIG. 6 shows transient responses due to the remote cylindrical boundary in the configuration of Fig. 5.

FIG. 7 shows transient responses in the presence of a remote boundary and a perfectly conductive metal pipe.

FIG. 8A, B show transient responses using pipes of differing conductivities.

FIG. 9 shows an unfiltered transient responses of data obtained in the presence of a conductive pipe.

FIG. 10 shows the data are of Fig. 9 subjected to least squares processing.

FIG. 11 shows the results of differential processing of the data of Fig. 9.

FIG. 12 shows the results of integral processing of the data of Fig. 9.

FIGS. 13A and 13B show the results of integral processing for pipes of varying conductivities.

FIG. 13C shows the transient responses in a conductive benchmark.

FIG. 13D shows the results of the integral processing of the responses shown in Fig. 13C.

DESCRIPTION OF PREFERRED EMBODIMENT

[0011] Figure 1 shows a schematic diagram of a drilling system 10 with a drillstring 20 carrying a drilling assembly 90 (also referred to as the bottom hole assembly, or "BHA") conveyed in a "wellbore" or "borehole" 26 for drilling the wellbore. The drilling system 10 includes a conventional derrick 11 erected on a floor 12 which supports a rotary table 14 that is rotated by a prime mover such as an electric motor (not shown) at a desired rotational speed. The drillstring 20 includes a tubing such as a drill pipe 22 or a

coiled-tubing extending downward from the surface into the borehole **26**. The drillstring **20** is pushed into the wellbore **26** when a drill pipe **22** is used as the tubing. For coiled-tubing applications, a tubing injector, such as an injector (not shown), however, is used to move the tubing from a source thereof, such as a reel (not shown), to the wellbore **26**. The drill bit **50** attached to the end of the drillstring breaks up the geological formations when it is rotated to drill the borehole **26**. If a drill pipe **22** is used, the drillstring **20** is coupled to a drawworks **30** via a Kelly joint **21**, swivel **28**, and line **29** through a pulley **23**. During drilling operations, the drawworks **30** is operated to control the weight on bit, which is an important parameter that affects the rate of penetration. The operation of the drawworks is well known in the art and is thus not described in detail herein.

[0012] During drilling operations, a suitable drilling fluid **31** from a mud pit (source) **32** is circulated under pressure through a channel in the drillstring **20** by a mud pump **34**. The drilling fluid passes from the mud pump **34** into the drillstring **20** via a desurger (not shown), fluid line **28** and Kelly joint **21**. The drilling fluid **31** is discharged at the borehole bottom **51** through an opening in the drill bit **50**. The drilling fluid **31** circulates uphole through the annular space **27** between the drillstring **20** and the borehole **26** and returns to the mud pit **32** via a return line **35**. The drilling fluid acts to lubricate the drill bit **50** and to carry borehole cutting or chips away from the drill bit **50**. A sensor S_1 preferably placed in the line **38** provides information about the fluid flow rate. A surface torque sensor S_2 and a sensor S_3 associated with the drillstring **20** respectively provide information about the torque and rotational speed of the drillstring. Additionally, a sensor (not shown) associated with line **29** is used to provide the hook load of the drillstring **20**.

[0013] In one embodiment of the invention, the drill bit **50** is rotated by only rotating the drill pipe **22**. In another embodiment of the invention, a downhole motor **55** (mud motor) is disposed in the drilling assembly **90** to rotate the drill bit **50** and the drill pipe **22** is rotated usually to supplement the rotational power, if required, and to effect changes in the drilling direction.

[0014] In the preferred embodiment of Figure **1**, the mud motor **55** is coupled to the drill bit **50** via a drive shaft (not shown) disposed in a bearing assembly **57**. The mud motor rotates the drill bit **50** when the drilling fluid **31** passes through the mud motor **55** under pressure. The bearing assembly **57** supports the radial and axial forces of the drill bit. A stabilizer **58** coupled to the bearing assembly **57** acts as a centralizer for the lowermost portion of the mud motor assembly.

[0015] In one embodiment of the invention, a drilling sensor module **59** is placed near the drill bit **50**. The drilling sensor module contains sensors, circuitry and processing software and algorithms relating to the dynamic drilling parameters. Such parameters preferably include bit bounce, stick-slip of the drilling assembly, backward rotation, torque, shocks, borehole and annulus pressure, acceleration measurements and other measurements of the drill bit condition. A suitable telemetry or communication sub **72** using, for example, two-way telemetry, is also provided as illustrated in the drilling assembly **90**. The drilling sensor module processes the sensor information and transmits it to the surface control unit **40** via the telemetry system **72**.

[0016] The communication sub **72**, a power unit **78** and an MWD tool **79** are all connected in tandem with the drillstring **20**. Flex subs, for example, are used in

connecting the MWD tool **79** in the drilling assembly **90**. Such subs and tools form the bottom hole drilling assembly **90** between the drillstring **20** and the drill bit **50**. The drilling assembly **90** makes various measurements including the pulsed nuclear magnetic resonance measurements while the borehole **26** is being drilled. The communication sub **72** obtains the signals and measurements and transfers the signals, using two-way telemetry, for example, to be processed on the surface. Alternatively, the signals can be processed using a downhole processor in the drilling assembly **90**.

[0017] The surface control unit or processor **40** also receives signals from other downhole sensors and devices and signals from sensors S_1 - S_3 and other sensors used in the system **10** and processes such signals according to programmed instructions provided to the surface control unit **40**. The surface control unit **40** displays desired drilling parameters and other information on a display/monitor **42** utilized by an operator to control the drilling operations. The surface control unit **40** preferably includes a computer or a microprocessor-based processing system, memory for storing programs or models and data, a recorder for recording data, and other peripherals. The control unit **40** is preferably adapted to activate alarms **44** when certain unsafe or undesirable operating conditions occur.

[0018] Figure 2A shows a typical cylindrical structure, comprising three zones substantially defined by a metal pipe **200**, adjacent transition layers **203**, and remote infinite formation **205**. Conductivities of the three zones are σ_1 , σ_2 , and σ_3 , respectively. The magnetic permeability of the entire space is μ . As illustrated, the cylindrical boundary **202** separating the metal pipe from the transition layer and the cylindrical

boundary **204** separating the regions of transition layer and remote formation share a common z -axis **210**. As measured from the z -axis, the radius of boundary **202** is labeled as r_{md} , and the radius of boundary **204** is labeled as r_{tl} . An electromagnetic field is excited by a transmitter current loop **215** of radius, r_{xt} , and is measured by a receiver loop **220** of radius r_{xr} . Transmitter loop and receiver loop are separated by distance L . The amplitude and frequency of the AC transmitter current are I and ω , respectively.

[0019] There is only one component E_ϕ of the electric field in the considered model of Fig. 2A, and it satisfies the Maxwell's equation detailed in Eq. (1) under the conditions of Eq. (2):

$$\frac{1}{r} \frac{\partial}{\partial r} \left(r \frac{\partial E_\phi}{\partial r} \right) - \frac{E_\phi}{r^2} + \frac{\partial^2 E_\phi}{\partial z^2} = k^2 E_\phi \quad (1)$$

$$\text{where } k_j^2 = -i\omega\mu\sigma_j, j = 1, 2, 3 \quad (2)$$

As is well known in the art, boundary conditions require a continuity of the tangential electric field E_ϕ , and of the tangential magnetic field, H_z , at boundaries **202** and **204**.

These conditions may be expressed mathematically in the form:

$$\left\{ \begin{array}{l} [E_\phi] = 0 \\ \left[\frac{\partial E_\phi}{\partial r} \right] = 0 \end{array} \right\} \text{ at } r = r_{md}, r_{tl} \quad (3)$$

An analytical solution for the boundary value problem of Eqs. (1) and (3), may be found using known techniques of the Fourier transform and separation of variables. The resulting expressions for an electromotive force induced in the receiver, $E_f = 2\pi r_{xt} E_\phi$, are shown below:

$$E_f = \int_0^\infty (F_a + F_b) \cos(\lambda L) d\lambda + \frac{i\omega\mu(2\pi r_{xt})(2\pi r_{xr})}{2\pi} \int_0^\infty \frac{\lambda}{2p_2} e^{-p_2 L} J_1(\lambda r_{xt}) J_1(\lambda r_{xr}) d\lambda \quad (4)$$

$$F_a = \frac{i\omega\mu(2\pi r_{xt})(2\pi r_{xr})}{2\pi^2 Det} \left[\begin{array}{l} \frac{I_1(p_2 * r_{md}) K_1(p_2 * r_{il})}{K_1(p_2 * r_{md}) I_1(p_2 * r_{il})} K_1(p_2 * r_{xt}) I_1(p_2 * r_{xt}) \frac{\alpha_{11}\alpha_{22}}{\alpha_{12}\alpha_{21}} \\ - \frac{K_1(p_2 * r_{il})}{I_1(p_2 * r_{il})} I_1(p_2 * r_{xt}) I_1(p_2 * r_{xr}) \frac{\alpha_{22}}{\alpha_{21}} \end{array} \right] \quad (5)$$

$$F_b = \frac{i\omega\mu(2\pi r_{xt})(2\pi r_{xr})}{2\pi^2 Det} \left[\begin{array}{l} \frac{I_1(p_2 * r_{md}) K_1(p_2 * r_{il})}{K_1(p_2 * r_{md}) I_1(p_2 * r_{il})} I_1(p_2 * r_{xt}) K_1(p_2 * r_{xt}) \frac{\alpha_{11}\alpha_{22}}{\alpha_{12}\alpha_{21}} \\ - \frac{I_1(p_2 * r_{md})}{K_1(p_2 * r_{md})} K_1(p_2 * r_{xt}) K_1(p_2 * r_{xr}) \frac{\alpha_{11}}{\alpha_{12}} \end{array} \right] \quad (6)$$

$$p_j^2 = k_j^2 + \lambda_j^2 \quad (7)$$

$$\alpha_{11} = 1 - \frac{p_2}{p_1} \frac{I_1(p_1 * r_{md}) I_0(p_2 * r_{md})}{I_0(p_1 * r_{md}) I_1(p_2 * r_{md})} \quad (8)$$

$$\alpha_{12} = 1 + \frac{p_2}{p_1} \frac{I_1(p_1 * r_{md}) K_0(p_2 * r_{md})}{I_0(p_1 * r_{md}) K_1(p_2 * r_{md})} \quad (9)$$

$$\alpha_{21} = 1 + \frac{p_2}{p_3} \frac{K_1(p_3 * r_{il}) I_0(p_2 * r_{il})}{K_0(p_3 * r_{il}) I_1(p_2 * r_{il})} \quad (10)$$

$$\alpha_{22} = 1 - \frac{p_2}{p_3} \frac{K_1(p_3 * r_{il}) K_0(p_2 * r_{il})}{K_0(p_3 * r_{il}) K_1(p_2 * r_{il})} \quad (11)$$

$$Det = 1 - \frac{I_1(p_2 * r_{md}) K_1(p_2 * r_{il}) \alpha_{11} \alpha_{22}}{K_1(p_2 * r_{md}) I_1(p_2 * r_{il}) \alpha_{12} \alpha_{21}} \quad (12)$$

The second term of Eq. (4) describes the field generated by a transmitter in an infinite uniform space with conductivity, σ_2 . The term F_a in Eq. (4) describes the field reflected from the boundary **204**. The coefficient, F_b , describes the field reflected from the inner boundary **202**.

[0020] Figure 3 shows a transmitter-receiver assembly lying next to a formation boundary 305. Transmitter and receiver lie along a common axis 301 that is horizontally positioned in the upper half-space 302 parallel to the formation boundary and is separated by a distance d from said boundary. The upper half-space 302 has a resistivity of 50 Ohm-m and the remote formation (lower half-space) 303 has a resistivity of 2 Ohm-m. Figure 4 shows transient responses of the transmitter-receiver assembly operated in the presence of a remote plane boundary without the presence of a metal pipe. Responses are measured in Volts along the vertical axis and the time is shown in seconds along the horizontal axis. The transmitter-receiver space is 2 m and transient responses are shown for several distances. Responses at distances of 1, 2, 4, 6, 8, and 10 meters are shown as 401, 402, 403, 404, 405, and 406, respectively. The response for infinite separation distance is shown as 407. Due to the skin-effect, at a very early times ($t < 100$ nanoseconds) there is no sensitivity to remote boundaries. In the time interval $100 \text{ nsec} < t < 100 \text{ } \mu\text{sec}$, the responses depend significantly on the distance to the boundary 305. It is during this time interval that the time when the currents diffuse deeper into formation and reach this boundary. Later, $t > 100 \text{ } \mu\text{sec}$, the responses once again show a lack of dependence on the distance to the boundary, because the diffusing currents have passed the boundary and are flowing predominantly in the conductive lower half-space 303.

[0021] Figure 5 introduces a cylindrical pipe into the model of Fig. 3. Introducing a cylindrical pipe into the considered formation introduces 3D effects. However, as in Fig. 5, one can consider a 1D cylindrically layer model where the inner layer 502 represents the 50 Ohm-m inner layer 302 (of Fig. 3) and the outer formation 504 has a resistivity of 2 Ohm-m. A more intense influence of the outer cylinder compared to the outer space in

a plane model of Fig. 3 is expected. Nevertheless, any approach developed for a cancellation of the pipe effect in a cylindrically layered formation will remain valid in the model with a plane boundary. Figure 6 shows the transient response in the presence of a remote cylindrical boundary without a metal pipe. The responses at a distance of 1, 2, 4, 6, 8, and 10 meters are shown as 601, 602, 603, 604, 605, and 606, respectively. The response for an infinite separation distance is shown as 607. Comparison of the responses in Fig. 6 to those in Fig. 4 indicate that the resolution in a cylindrical geometry is larger than the resolution obtained from a plane model. Such resolution is, however, sufficient for boundary detection. A greater separation can be found between curves 601 through 606 than are found between curves 401 through 407. The separation of response curves is most pronounced at earlier times in Fig. 6.

[0022] The ability of the method of the present invention to obtaining a temporal signal substantially independent of conductivity enables for a reduced distance between transmitter and receiver. Typical prior art methods requires transmitter-receiver spacing in a range of 20-30m in order to obtain a measurement at a radial depth of about 10m. In the method of present invention, the same depth can be achieved with a spacing of 1-2m. The sensitivity to remote formation volumes is substantially independent of transmitter-receiver spacing.

[0023] It is possible to use the general model of Fig. 2A to obtain equations under more specific conditions. For example, Figure 2B shows the model from Figure 2A under the condition of a perfectly conductive pipe $\sigma_1 = \infty$ and with $\sigma_2 = \sigma_3$. When $\sigma_2 = \sigma_3$, it follows from Eq. (11) that the coefficient a_{22} , vanishes and, consequently $F_a = 0$

(see Eq. 5). The generalized equations above are subsequently simplified to Eqs. (13) and (14) shown below:

$$E_f = \int_0^{\infty} (F_b) \cos(\lambda L) d\lambda + \frac{i\omega\mu(2\pi r_{xt})(2\pi r_{xr})}{2\pi} \int_0^{\infty} \frac{\lambda}{2p_2} e^{-p_2 L} J_1(\lambda r_{xt}) J_1(\lambda r_{xr}) d\lambda \quad (13)$$

where

$$F_b = \frac{i\omega\mu(2\pi r_{xt})(2\pi r_{xr})}{2\pi^2} \left[\frac{I_1(p_2 * r_{md})}{K_1(p_2 * r_{md})} K_1(p_2 * r_{xt}) I_1(p_2 * r_{xr}) \right] \quad (14)$$

These equations describe the frequency dependence of the measured field for all frequencies of the transmitter current (for $I=1$ Ampere). The second term of the Eq. (13) describes the electromotive force in a uniform space with conductivity, σ_2 (primary field). The first term represents the effect of the pipe (secondary field). The transient response of this perfectly conducting pipe with a remote boundary is shown in Figure 7. The time duration is measured on the horizontal axis from 10^{-8} seconds to 10^{-2} seconds. The response is measured in Volts. Response curves obtained distances $d = 1, 2, 4, 6, 8$, and 10 meters are shown as **701, 702, 703, 704, 705, and 706**. The response obtained at an infinite separation distance is shown as **707**. The separation of the curves indicates that the measured field retains a high sensitivity to remote boundaries even in the presence of a perfectly conductive pipe. Comparison of **Figs. 6 and 7** shows that they are substantially identical.

[0024] An expansion of the local fields can be made in the frequency domain. The electric field, \mathbf{E} , may be expanded in the following Taylor series with respect to $\frac{1}{2}$ powers of the frequency ω .

$$E = \sum_{k=2}^{k=\infty} u_{k/2} (-i\omega)^{k/2} \quad (15)$$

$$u_{3/2} = 0$$

The coefficient $u_{5/2}$ corresponding to the term $\omega^{5/2}$ is independent of the properties of a near borehole zone, thus $u_{5/2} = u_{5/2}^0$. Rather this term is sensitive only to the conductivity distribution in the undisturbed formation.

[0025] The magnetic field can similarly be expanded in a Taylor series (16):

$$H = \sum_{k=0}^{k=\infty} s_{k/2} (-i\omega)^{k/2} \quad (16)$$

$$s_{1/2} = 0$$

The coefficient $s_{3/2}$ of the term corresponding to $\omega^{3/2}$ can be shown to depend only on the properties of the background formation, in other words $s_{3/2} = s_{3/2}^0$.

[0026] Referring to Eq. (A3.9) of the Appendix, in the frequency domain, Eq. (17), below, accounts for the finite conductivity of the pipe if the shape of the applied current is assumed to be the Dirac function, $\delta(t)$:

$$H(\omega) = H^0(\omega) + \frac{1}{\sqrt{\sigma_c}} \left(\frac{b_0}{(-i\omega\mu)^{1/2}} + (-i\omega\mu)^{1/2} b_1 + (-i\omega\mu) b_{3/2} + (-i\omega\mu)^{3/2} b_2 + \dots \right) \quad (17)$$

where H is the measured magnetic field in the presence of a finite conductivity pipe; H^0 is the magnetic field that would be measured if the pipe were perfectly conductive; σ_c is the conductivity of the pipe; $\omega = 2\pi f$, where f is the frequency; and μ is the magnetic permeability of the free space. This expansion can be transferred to the time domain to obtain an expression of the transient field response. Transformation of the Eq. (17) to the time domain using the Fourier transform yields:

$$H(t) \approx H^0(t) + \frac{1}{\sqrt{\sigma_c}} \frac{1}{\sqrt{\pi}} \left(\frac{1}{(t\mu)^{1/2}} b_0 - \frac{\mu^{1/2}}{2t^{3/2}} b_1 + \frac{3\mu^{3/2}}{4t^{5/2}} b_2 + \dots \right) \quad (18)$$

In the absence of a pipe, the measured electromotive force for step-function switch-on/switch-off modes, or the equivalent H_z^0 component of the magnetic field for the Dirac current shape, have the following expansion

$$H_z^0 \approx \frac{(H_z^0)_{5/2}}{t^{5/2}} + \frac{(H_z^0)_{7/2}}{t^{7/2}} + \dots \quad (19)$$

A comparison of Eq. (17) and Eq. (18) shows that the following correspondence exists between the frequency series and the time domain expansion of the field at late times (for step-function switch-on/switch-off modes):

$$t^{-n/2} \Rightarrow \omega^{n/2-1}, n = 1, 3, 5, \dots \quad (20)$$

The integer powers of the frequency expansions do not contribute to the late stage of the transient process.

[0027] Terms that are on the order of $\omega^{3/2}$ correspond to the terms that are on the order of $t^{-5/2}$ in the transient domain. Collecting these terms leads to Eq. (21) below:

$$\frac{(H_z)_{3/2}}{t^{5/2}} \approx \frac{(H_z^0)_{3/2}}{t^{5/2}} + \frac{1}{\sqrt{\sigma_c}} \frac{3\mu^{3/2}}{4\sqrt{\pi}} \frac{b_2}{t^{5/2}} \quad (21)$$

In order to obtain time domain results comparable with multi-frequency focusing (MFF), an elimination of the terms in $t^{-1/2}$ and $t^{-3/2}$ in Eq. (18) is practical.

[0028] The structure of the expansion (18) enables the following general trends in the behavior of the transient response when the conductivity of the pipe is finite but large:

- As time increases, the signal due to the pipe dominates over the signal generated by the formation. The dominance occurs because the formation response decays much faster ($t^{-5/2}$) compared to the pipe response ($t^{-1/2}$). Increasing the pipe contribution to the measured field results in a reduced sensitivity to remote boundaries.
- The higher the conductivity of the pipe, the less the effect of the pipe on the resolution, because the terms describing the pipe signal are inversely proportional to $\sigma^{1/2}$.

[0029] The present invention removes the effects of term $t^{-1/2}$ and $t^{-3/2}$. Typically, coefficient b_0 can be determined by examining the signal at a time late in the transient behavior (in the range of 10^{-4} to 10^{-2}). As terms of $t^{-5/2}$ and higher decay at earlier times, data at all varying transmitter-receiver distances exhibit the same tail end behavior.

[0030] Figure 8A shows the transient responses obtained in the presence of a typical conductive pipe. The conductivity is $\sigma=1.4*10^6$ S/m. Curves 801, 802, and 803, indicate responses at distances of 1, 2, and 4 meters to a remote boundary. Response curve 804 represents the response to a remote boundary at an infinite distance. Response curve 804 is nearly indistinguishable from and overlaps response curves at a distance of 6m, 8m, and 10m. Increasing the conductivity of the metal pipe improves the sensitivity of the tool to a remote boundary. Fig. 8B shows the transient responses for a tool with an increased conductivity of the pipe, $\sigma=1.4*10^{10}$ S/m, taken at various distances to the remote boundary. The σ of the pipe of Fig. 8B is 4 orders of magnitude higher than the

typical conductivity of a metal pipe of Fig. 8A. The response curves of Fig. 8B reflects an improvement in sensitivity. Curves 811, 812, 813, 814, 815, and 816 represent the response to a remote boundary at a distance of 1, 2, 4, 6, 8, and 10 meters, respectively. Curve 817 represents the response to a remote boundary at an infinite distance. Comparing the curves of Fig. 8B to the curves of Fig. 8A, it is possible to observe a significant increase in the spread in the magnitude of the response curves 811 through 816 in Fig. 8B to that of the response curves 801 through 804 in Fig. 8A.

[0031] The present invention outlines several numerical methods for correcting measurements obtained in the presence of a pipe with finite conductivity. The asymptotic Eq. (18) indicates that, within certain time intervals, the electromotive transient magnetic field may be expanded in the following Taylor series expansion:

$$\begin{pmatrix} H_z(t_1) \\ H_z(t_2) \\ \vdots \\ H_z(t_{m-1}) \\ H_z(t_m) \end{pmatrix} = \begin{pmatrix} t_1^{-1/2} & t_1^{-3/2} & t_1^{-5/2} & \bullet & \bullet & \bullet & t_1^{n/2} \\ t_2^{-1/2} & t_2^{-3/2} & t_2^{-5/2} & \bullet & \bullet & \bullet & t_2^{n/2} \\ \bullet & \bullet & \bullet & \bullet & \bullet & \bullet & \bullet \\ \bullet & \bullet & \bullet & \bullet & \bullet & \bullet & \bullet \\ \bullet & \bullet & \bullet & \bullet & \bullet & \bullet & \bullet \\ t_{m-1}^{-1/2} & t_{m-1}^{-3/2} & t_{m-1}^{-5/2} & \bullet & \bullet & \bullet & t_{m-1}^{n/2} \\ t_m^{-1/2} & t_m^{-3/2} & t_m^{-5/2} & \bullet & \bullet & \bullet & t_m^{n/2} \end{pmatrix} \begin{pmatrix} S_{1/2} \\ S_{3/2} \\ S_{5/2} \\ \bullet \\ \bullet \\ \bullet \\ S_{(2n-1)/2} \end{pmatrix} \quad (22)$$

where t_1, \dots, t_m is the measurement time, and $s_{1/2}, \dots, s_{n/2}$ are the expansion coefficients.

[0032] A comparison of Eqs. (18), (19) and (22), reveals that coefficients, $S_{1/2}$ and $S_{3/2}$, are mostly dependent on the pipe conductivity. Only the third expansion coefficient $S_{5/2}$ is directly related to the formation conductivity (see Eq. 21):

$$S_{5/2} = (H_z^0)_{S_{5/2}} + \frac{1}{\sqrt{\sigma_c}} \frac{3\mu^{3/2}}{4\sqrt{\pi}} b_2 \quad (23)$$

Given a sufficient measurement time ($m > n$), one can find the least squares solution for the system of Eq. (22) and preferably subtract the terms corresponding to $S_{1/2}$ from the measured field to remove effects of pipe conductivity. Numerical modeling confirms that, for all practical purposes, it is satisfactory to cancel only the $S_{1/2}$ term.

Alternatively, and depending on the pipe and formation conductivity, one can calculate both the effects of $S_{1/2}$ and $S_{3/2}$ in Eq. (22) and Eq. (24):

$$\tilde{H}(t) = H_z(t) - \frac{S_{1/2}}{t^{1/2}} - \frac{S_{3/2}}{t^{3/2}} \quad (24)$$

where H_z is the measured response. Figure 9 shows a transient behavior of data prior to processing. Reference numerals **901**, **902**, and **903**, indicate responses at distances of 1, 2, and 4 meters to a remote boundary. Response curve **904** represents the response to a remote boundary at distances of 6m, 8m, 10m, or an infinite distance. These response curves are nearly indistinguishable from each other. In Figure 10, the data of Figure 9 are subjected to the least square processing of Eq. (22). The resolution is thereby significantly improved. Separation can be seen between response curves **1001**, **1002** and **1003** representing response to a remote boundary at 1, 2, and 4 meters. Furthermore response curves **1004**, **1005**, and **1006**, representing responses to a remote boundary at 6, 8, and 10 meters, are distinguishable from each other and from curve **1007**, which represents a boundary at infinite distance.

[0033] Alternatively, Eq. (18) enables the construction of several localized filters for eliminating the pipe influence. Typically, these filters comprise small sliding windows. Filtering can be performed using differentiation or integration methods. The following filter of Eq. (25) eliminates the main term b_0 , of the pipe contribution:

$$H_z^{dif} = \frac{\partial(t^{1/2} H_z)}{\partial t} \quad (25)$$

where H_z is the measured response. Figure 11 shows the results of differential processing of the curves of Fig. 9. For time durations less than 10^{-4} seconds, response curves can be distinguished from each other. Curves 1101, 1102, 1103, 1104, 1105 and 1106 represent responses to a remote boundary at a distance of 1, 2, 4, 6, 8, and 10 meters. Curve 1107 represents a response to a remote boundary at an infinite distance. Comparison with Fig. 9 indicated an improved resolution.

[0034] In order to filter using integration, it is practical to consider two times, t_1 and t_2 . An average of the measured field with a weight of $t^{1/2}$ can be made over two time intervals, both having a duration Δ . The first and the second intervals are centered at the points, t_1 and t_2 , respectively. Integrating over the time interval, one obtains:

$$I_1 = \frac{1}{\Delta} \int_{-\Delta/2}^{\Delta/2} t^{1/2} H_z(t-t_1) dt \approx \frac{1}{\Delta} \int_{-\Delta/2}^{\Delta/2} t^{1/2} H_z^0(t-t_1) dt + \frac{b_0}{\sqrt{\pi\mu\sigma_c}} \quad (26)$$

$$I_2 = \frac{1}{\Delta} \int_{-\Delta/2}^{\Delta/2} t^{1/2} H_z(t-t_2) dt \approx \frac{1}{\Delta} \int_{-\Delta/2}^{\Delta/2} t^{1/2} H_z^0(t-t_2) dt + \frac{b_0}{\sqrt{\pi\mu\sigma_c}} \quad (27)$$

The difference of Eq. (26) and (27) produces an integration filter Eq. (28) that eliminates the influence of the pipe:

$$I_1 - I_2 \approx \frac{1}{\Delta} \int_{-\Delta/2}^{\Delta/2} t^{1/2} [H_z^0(t-t_1) - H_z^0(t-t_2)] dt \quad (28)$$

Figure 12 shows the results of integral processing of the data of Fig. 9. Pipe conductivity is 1.4×10^6 S/m. Curves 1201, 1202, 1203, 1204, 1205 and 1206 represent responses to a remote boundary at a distance of 1, 2, 4, 6, 8, and 10 meters. Curve 1207 represents a

response to a remote boundary at an infinite distance. Both differential and integration processing result in a resolution improvement. Processing via integration is typically more stable.

[0035] Figures 13A and 13B show the results of integral processing for more conductive pipes. Fig. 13A shows a pipe conductivity equal to 3×10^7 S/m. Curves 1301, 1302, 1303, 1304, 1305 and 1306 represent responses to a remote boundary at a distance of 1, 2, 4, 6, 8, and 10 meters. Curve 1307 represents a response to a remote boundary at an infinite distance. Fig. 13B shows a pipe conductivity equal to 1.4×10^{10} S/m. Curves 1311, 1312, 1313, 1314, 1315 and 1316 represent responses to a remote boundary at a distance of 1, 2, 4, 6, 8, and 10 meters. Curve 1317 represents a response to a remote boundary at an infinite distance. The filtered signal does not depend on the pipe conductivity at earlier times. At later times, the pipe makes a dominant contribution to the measured signal, and this is reflected in the loss of resolution.

[0036] Fig. 13C shows the response for 2-meter spacing of a more conductive formation. Curves 1321, 1322, and 1323 represent responses to a remote boundary at a distance of 1, 2, and 4 meters. Response curve 1327 represents the response to a remote boundary at an infinite distance. Response curves at distances of 6m, 8m, and 10m are indistinguishable from curve 1327. These response curves are nearly indistinguishable from each other. Results shown in the figure ensure that, on the low resistivity end, the response retains the necessary sensitivity. The formation resistivity is changed to 10 Ohm-m and the shale/water resistivity to 1 Ohm-m. Comparing Fig. 13C to Fig. 9, one can observe the skin-effect in Fig. 13C at very early times (i.e. 10^{-8} sec) and the shift of

maximum sensitivity ($\sim 3 \cdot 10^{-7}$ sec in Fig. 9) to later times ($\sim 10^{-6}$ sec in Fig. 13C). Both facts can be explained due to an increase of the formation conductivity.

[0037] In Fig. 13D, results of the integral processing are presented. Curves 1331, 1332, 1333, 1334, 1335 and 1336 represent responses to a remote boundary at a distance of 1, 2, 4, 6, 8, and 10 meters. Curve 1337 represents a response to a remote boundary at an infinite distance. Comparison of Fig. 13D with Fig. 12 shows a time period of maximum sensitivity of the processed data being shifted to later times. (See, for example, curves 1201 through 1204 in Fig. 12 and curves 1331 through 1334 in Fig. 13D) This maximum sensitivity has the same order of magnitude as the sensitivity of the processed data in the resistive benchmark.

[0038] The invention has been described above with reference to a MWD apparatus carried on a drillstring. The method of the invention can also be used on other types of MWD apparatus conveyed on a drilling tubular, and may also be used on a logging tool carried on a wireline. The last such method is of relatively minor importance since on wireline devices, it is possible to have a housing of very high conductivity so that the correction methods described herein may not be necessary. Such means of conveyance would be known to those versed in the art and are not discussed further.

[0039] While the foregoing disclosure is directed to the preferred embodiments of the invention, various modifications will be apparent to those skilled in the art. It is intended that all such variations within the scope and spirit of the appended claims be embraced by the foregoing disclosure.

APPENDIX: TAYLOR'S FREQUENCY SERIES FOR MWD ELECTROMAGNETIC TOOL

[0040] We intend to evaluate the asymptotic behavior of magnetic field on the surface of a metal mandrel as described in Eq. (6):

$$H_{\alpha}(P) = H_{\alpha}^0(P) + \beta \int_S \left\{ \vec{H}^{M\alpha} \vec{h} \right\} dS \quad (A3.1)$$

where $H_{\alpha}(\mathbf{P})$ is the magnetic field measure along the direction α (α -component), \mathbf{P} is the point of measurement, $H_{\alpha}^0(\mathbf{P})$ is the α -component of the measured magnetic field given a perfectly conducting mandrel, S is the surface of the tool mandrel, $\beta = 1/\sqrt{-i\omega\mu\sigma_c}$,

where ω and μ are frequency and magnetic permeability, and ^{Ma}h is the magnetic field of an auxiliary magnetic dipole in a formation where the mandrel of a finite conductivity is replaced by an identical body with a perfect conductivity. The dipole is oriented along α -direction. At high conductivity, β is small. The primary and auxiliary magnetic fields, H_{α}^0 and ^{Ma}h , depend only on formation parameters. The total magnetic field, H_{α} , depends on both formation parameters and mandrel conductivity. The dependence on mandrel conductivity, σ_c , is reflected only in parameter β :

$$\beta = \frac{1}{k_c} = \frac{1}{\sqrt{-i\omega\mu\sigma_c}} \quad (A3.2)$$

The perturbation method applied to Eq.(A3.1) leads to the following result:

$$H_{\alpha} = \sum_{i=0}^{i=\infty} {}^{(i)}H_{\alpha} \quad (A3.3)$$

$$^{(0)}H_{\alpha} = H_{\alpha}^0 \quad (\text{A3.4})$$

$$^{(i)}H_{\alpha} = \beta \int_S \left\{ ^{(i-1)}\bar{H}^{M\alpha} \bar{h} \right\} dS \quad (\text{A3.5})$$

$$i = 1, \dots, \infty$$

[0041] Let us consider the first order approximation that is proportional to the parameter β :

$$^{(1)}H_{\alpha} = \beta \int_S \left\{ ^{(0)}\bar{H}^{M\alpha} \bar{h} \right\} dS = \beta \int_S \left\{ \bar{H}_0^{M\alpha} \bar{h} \right\} dS \quad (\text{A3.6})$$

The integrand in Eq. (A3.6) does not depend on mandrel conductivity. Therefore, the integral in right-hand side, Eq. (A3.6), may be expanded in wireline-like Taylor series with respect to the frequency:

$$\int_S \left\{ \bar{H}_0^{M\alpha} \bar{h} \right\} dS \approx b_0 + (-i\omega\mu)b_1 + (-i\omega\mu)^{3/2}b_{3/2} + (-i\omega\mu)^2b_2 + \dots \quad (\text{A3.7})$$

In axially symmetric models, coefficients b_j have the following properties:

- b_0 does not depend on formation parameters. It is related to so called ‘direct field’;
- b_1 is linear with respect to formation conductivity. It is related to Doll’s approximation;
- $b_{3/2}$ depends only on background conductivity and does not depend on near borehole parameters;
- b_2 includes dependence on borehole and invasion.

[0042] Let us substitute Eq.(A3.7) into Eq.(A3.6):

$$^{(1)}H_{\alpha} = \frac{1}{\sqrt{\sigma_c}} \left(\frac{b_0}{(-i\omega\mu)^{1/2}} + (-i\omega\mu)^{1/2} b_1 + (-i\omega\mu) b_{3/2} + (-i\omega\mu)^{3/2} b_2 + \dots \right) \quad (\text{A3.8})$$

Eq.(A3.3), (A3.4), and (A3.8) yield:

$$H_{\alpha} \approx H_{\alpha}^0 + \frac{1}{\sqrt{\sigma_c}} \left(\frac{b_0}{(-i\omega\mu)^{1/2}} + (-i\omega\mu)^{1/2} b_1 + (-i\omega\mu) b_{3/2} + (-i\omega\mu)^{3/2} b_2 + \dots \right) \quad (\text{A3.9})$$

Collecting traditionally measured in MFF terms $\sim\omega^{3/2}$, we obtain:

$$(-i\omega\mu)^{3/2} (H_{\alpha})_{3/2} \approx (-i\omega\mu)^{3/2} (H_{\alpha}^0)_{3/2} + \frac{(-i\omega\mu)^{3/2} b_2}{\sqrt{\sigma_c}} \quad (\text{A3.10})$$

The first term in the right hand side, Eq.(A3.10), depends only on background formation.

The presence of imperfectly conducting mandrel makes the MFF measurement dependent also on a near borehole zone parameters (second term, coefficient b_2) and mandrel conductivity, σ_c . This dependence, obviously, disappears for a perfect conductor ($\sigma_c \rightarrow \infty$). We should expect a small contribution from the second term since conductivity σ_c is very large.

[0043] To measure the term $\sim\omega^{3/2}$, we can modify MFF transformation in such a way that contributions proportional to $1/(-i\omega\mu)^{1/2}$ and $(-i\omega\mu)^{1/2}$, Eq. (A3.9), are cancelled. We also can achieve the goal by compensating the term $\sim 1/(-i\omega\mu)^{1/2}$ in the air and applying MFF to the residual signal. The latter approach is preferable because it improves the MFF stability (less number of terms needs to be compensated). Let us consider a combination of compensation in the air and MFF in more detail. It follows from Eq. (A3.9) that the response in the air, $H_{\alpha}(\sigma=0)$, may be expressed in the following form:

$$H_a(\sigma = 0) \approx H_a^0(\sigma = 0) + \frac{1}{\sqrt{\sigma_c}} \left(\frac{b_0}{(-i\omega\mu)^{1/2}} \right) \quad (A3.11)$$

Compensation of the term $\sim b_0$, Eq.(A3.11), is critical. Physically, this term is due to *strong currents on the conductor surface* and its contribution (not relating to formation parameters) may be very significant. Equations (A3.9) and (A3.11) yield the following compensation scheme:

$$H_a - H_a(\sigma = 0) \approx (-i\omega\mu)(H_a)_1 + (-i\omega\mu)^{3/2}(H_a)_{3/2} + \frac{1}{\sqrt{\sigma_c}} \left((-i\omega\mu)^{1/2} b_1 + (-i\omega\mu) b_{3/2} + (-i\omega\mu)^{3/2} b_2 + \dots \right) \quad (A3.12)$$

Considering measurement of imaginary component of the magnetic field, we obtain:

$$\text{Im}[H_a - H_a(\sigma = 0)] \approx - \left\{ \frac{1}{\sqrt{\sigma_c}} \left(\frac{\omega\mu}{\sqrt{2}} \right)^{1/2} b_1 + \omega\mu(H_a)_1 + \left(\frac{\omega\mu}{\sqrt{2}} \right)^{3/2} \left((H_a)_{3/2} + \frac{b_2}{\sqrt{\sigma_c}} \right) \right\} \quad (A3.13)$$

)

[0044] Equation (A3.13) indicates that in MWD applications, two frequency terms must be cancelled as opposed to only one term in wireline. Equation, (A1.4), modified for MWD applications has the following form:

$$\begin{pmatrix} H(\omega_1) \\ H(\omega_2) \\ \vdots \\ \vdots \\ H(\omega_{m-1}) \\ H(\omega_m) \end{pmatrix} = \begin{pmatrix} \omega_1^{1/2} & \omega_1^1 & \omega_1^{3/2} & \omega_1^{5/2} & \bullet & \bullet & \bullet & \omega_1^{n/2} \\ \omega_2^{1/2} & \omega_2^1 & \omega_2^{3/2} & \omega_2^{5/2} & \bullet & \bullet & \bullet & \omega_2^{n/2} \\ \bullet & \bullet & \bullet & \bullet & \bullet & \bullet & \bullet & \bullet \\ \bullet & \bullet & \bullet & \bullet & \bullet & \bullet & \bullet & \bullet \\ \bullet & \bullet & \bullet & \bullet & \bullet & \bullet & \bullet & \bullet \\ \omega_{m-1}^{1/2} & \omega_{m-1}^1 & \omega_{m-1}^{3/2} & \omega_{m-1}^{5/2} & \bullet & \bullet & \bullet & \omega_{m-1}^{n/2} \\ \omega_m^{1/2} & \omega_m^1 & \omega_m^{3/2} & \omega_m^{5/2} & \bullet & \bullet & \bullet & \omega_m^{n/2} \end{pmatrix} \begin{pmatrix} s_{1/2} \\ s_1 \\ s_{3/2} \\ s_{5/2} \\ \bullet \\ \bullet \\ \bullet \\ s_{n/2} \end{pmatrix} \quad (A3.14)$$

The residual signal (third term) depends on the mandrel conductivity but the examples considered in the report illustrate that this dependence is negligible due to very large

conductivity of the mandrel. Similar approaches may be considered for the voltage measurements.